LH Transition by a Biased Hot Cathode in the Tohoku University Heliac

S. Kitajima 1), H. Takahashi 1), Y. Tanaka 1), H. Utoh 1), M. Sasao 1), M. Takayama 2), K. Nishimura 3), S. Inagaki 3) and M. Yokoyama 3)

1) Department of Quantum Science and Energy Engineering, Tohoku University, Sendai, 980-8579, Japan
2) Akita Prefectural University, Honjyo, Akita, 015-0055, Japan
3) National Institute for Fusion Science, Toki, Gifu 509-5292, Japan

e-mail:sumio.kitajima@qse.tohoku.ac.jp

Abstract. In the Tohoku University Heliac (TU-Heliac), a helical axis stellalator, the transition mechanism to an improved mode has been intensively studied by biasing experiments using a hot cathode of LaB_6. The negative electrode biasing by a hot cathode triggered an improved confinement mode, and the bifurcation phenomena, *i.e.*, a negative resistance feature in the electrode characteristics that accompanies this L-H transition, were observed. The ion viscous damping force was estimated from the $\boldsymbol{J} \times \boldsymbol{B}$ driving force for the poloidal rotation and the effects of the local maxima on ion viscosity were investigated. The measured damping forces agreed well with those of the neoclassical theory, and had a local maximum at the poloidal Mach number $M_p \sim 1.5$ where the neoclassical theory predicts a local maximum originated from a toroidal ripple. The plasma showed negative resistance characteristics in the region where the neoclassical ion viscous damping force had a local maximum.

1. Introduction

Although the H-mode is widely observed in both tokamaks and stellarators [1-5], there are few universal characteristics in helical/stellarator devices. One of the reasons is that each of stellarators has its own Fourier components of the magnetic field, causing the complexity in radial particle fluxes and in the ion viscous force. In theories for L-H transition, the local maximum in ion viscosity against poloidal Mach number M_p around $-M_p \sim 1\text{-}3$ is considered to play the key role [6-9]. This maximum is considered to be related to the toroidicity, hence, a universal feature among tokamaks and stellarators can be studied if this region is investigated in detail. Electrode-biasing experiments are one of effective tools for the study of improved confinement modes [10-13]. In our previous experiments on the Tohoku University Heliac (TU-Heliac)[14], a cold electrode and a constant voltage power supply was used and an improved mode was successfully triggered as a transition to a high-density region when $M_p >$ 1. The measured dumping force showed a local maximum at M_p =1-2. However, the driving force for plasma rotation was not controlled continuously with this set-up. On the other hand, the non-linearity of plasma viscosity was investigated using a cold electrode with a voltage-sweep biasing in IMS [15]. They clearly showed that the non-linearity of plasma viscosity at $-M_p \sim 20$, but improvement of plasma confinement was not reported. In the present experiments we adopted an electron-injection-hot-cathode as a biasing electrode to control the driving force for plasma rotation externally and it was drived by a current-control power supply. The measurement of the poloidal rotation may allow estimation of ion viscous damping force. The purposes of our electrode biasing experiments were, (1) to study the characteristics of biased plasmas in TU-Heliac, (2) to study the feasibility of active control of the driving force for the poloidal rotation by a hot cathode, (3) to estimate the ion viscous damping forces from the driving forces in a wide range of collisionality, and (4) to perform a comparison between the measured ion viscous damping force and the neoclassical predictions [8, 16].

2. Characteristics of a Biased Plasmas with *Constant Voltage*

The TU-Heliac is a 4-period heliac (major radius, 0.48 m; average plasma radius, 0.07 m) [14,

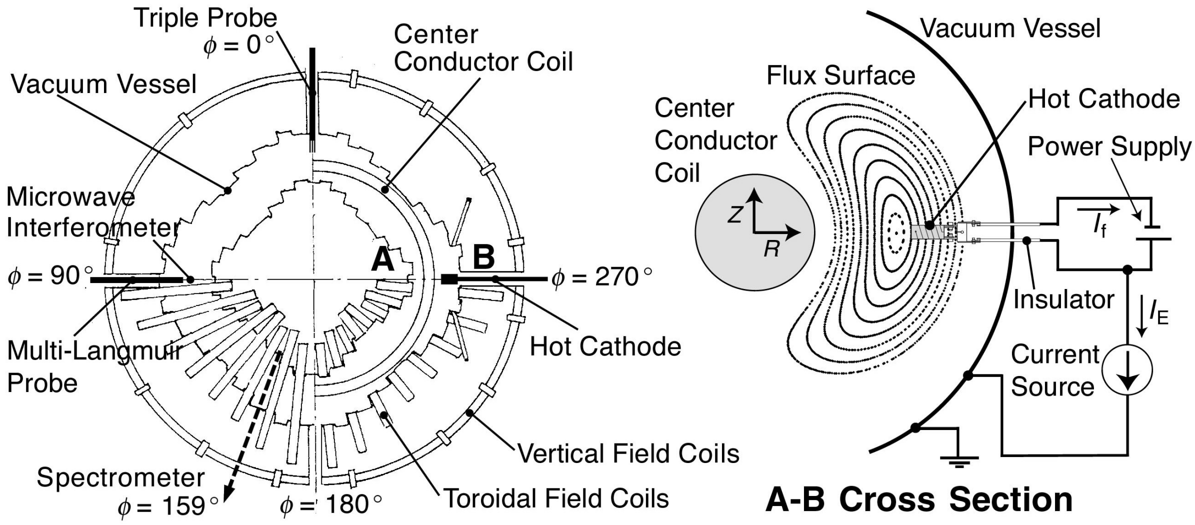

FIG. 1. The Experimental setup.

17]. The heliac configurations were produced by three sets of magnetic field coils: 32 toroidal field coils, a center conductor coil, and one pair of vertical field coils. Three capacitor banks consisting of two-stage pulse forming networks separately supplied coil currents of 10 msec flat top. The target plasma for biasing was He plasma produced by low frequency joule heating (f = 18.8 kHz, P_{out} ~ 35 kW). The joule heating power was supplied to one pair of poloidal coils wound outside the toroidal coils [18]. The vacuum vessel was filled with fueling neutral He gas and sealed before every discharge.

The electrode biasing experiments were carried out in the TU-Heliac using an emissive hot cathode made of LaB_6, which functions as an electron injection source. The LaB_6 hot cathode (diameter, 10 mm; length, 17 mm) was inserted horizontally into the plasma from the low field side at a toroidal angle ϕ = 270° as shown in Fig. 1. In a poloidal cross-section, the flux surface was bean or kidney shaped. The hot cathode was heated by a floating power supply and negative bias voltage or negative current source was applied against the vacuum vessel by a *voltage-control* or *current-control* power supply (Fig. 1). The radial profiles of electron temperature, density, plasma potential, and these fluctuation levels were measured by a triple probe at a toroidal angle ϕ = 0°. The line density along a vertical chord through the magnetic axis was measured by a 6 mm microwave interferometer at ϕ = 90°. The poloidal distribution of fluctuation levels were measured by multi Langmuir probes that were aligned along a magnetic surface at ϕ = 90°. The visible light emission was monitored by a 25 cm spectrometer at ϕ = 159°. The typical plasma parameters before biasing were as follows. The electron density on the magnetic axis was 6×10^{11} cm^{-3} and the electron temperature on the axis was about 25 eV. The magnetic field on the axis was 0.3 T.

First, we examined the characteristics of biased plasmas in the TU-Heliac with *constant voltage* biasing experiments. Figure 2 shows the typical time evolution of the electrode voltage V_E, the electrode current I_E, and the plasma parameters. In this experiment, the negative bias voltage was applied against the vacuum vessel by a *constant-voltage* power supply. Figure 2

(c) shows radial electric fields estimated from the potential profiles measured by the triple probe at three different adjacent radial points. Here, ρ is the averaged radius normalized by the averaged radius of the last closed flux surface. It is clear that the biased electrode induced a strong negative radial electric field and a radial electric field shear. This field was initially formed near the magnetic axis and then extended toward the plasma boundary. After formation of the electric field, the line density measured by the interferometer increased by a factor of 2 ~ 3 (Fig. 2 (d)), the fluctuation level of the floating potential and that of the ion saturation current measured by the triple probe were suppressed (f), (g), and the impurity light emission (H_α) normalized by $n_e\langle\sigma v\rangle$ decreased (h), where n_e is the electron density and $\langle\sigma v\rangle$ is the rate coefficient of the electron excitation [19]. The radial profile measurements obtained by the triple probe also indicated that the electron density profile steepened during biasing [20].

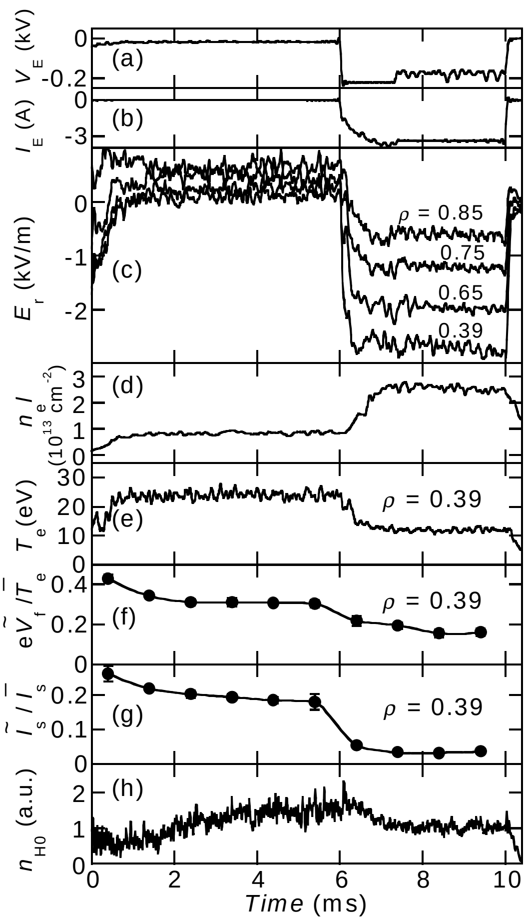

FIG. 2. Typical time evolution of (a) electrode voltage, (b) electrode current, (c) radial electric fields, (d) electron line density, (e) electron temperature, (f) floating potential fluctuation level, (g) ion saturation current fluctuation level, and (h) impurity light emission normalized by $n_e\langle\sigma v\rangle$. The normalized radius is indicated by ρ.

Previously [21], we actively changed the electrode voltage. The stored energy is plotted against the hot cathode input power in Fig. 3. The input power of the low frequency joule heating was kept constant. The stored energy was estimated from the product of the density and the electron temperature. The linear gradient after the formation of the electric field was about twice larger than that before the formation. This suggests the energy confinement time increases by a factor of 2. These observations indicated that the TU-Heliac shows the same characteristics as the H-mode in large tokamaks and stellarators.

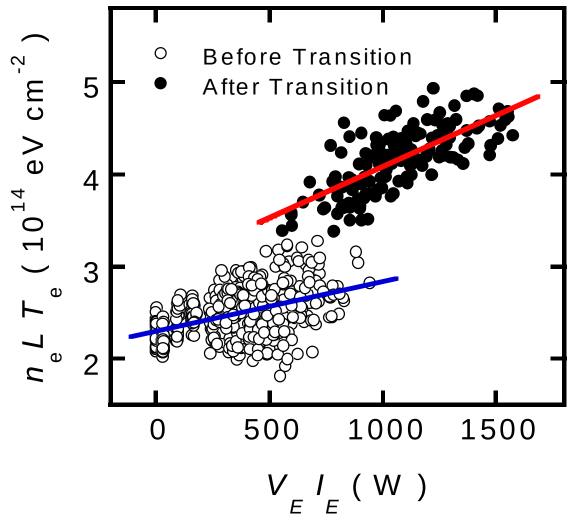

FIG. 3. The stored energy dependence on the electrode input power.

3. Feasibility Study of Active Control of the Driving Force with *Current Sweep*

The feasibility of active control of the driving force for the poloidal rotation was examined by sweeping the electrode current with an external control signal.

Figure 4 shows typical time evolution of (a) the electrode current, (b) the electrode voltage, (c) radial electric fields, (d) electron line density, (e) electron temperature, (f) floating potential fluctuation level and (g) ion saturation current fluctuation level. In this experiment, the electrode current was kept constant at ~ 4 ampere from 0 to 5 msec and then ramped down from 5 to 10 msec, as is shown in (a). The electric fields in outer region (c) decreased gradually by the current-control power supply, indicating the capability of active control of the driving force for the poloidal rotation. In the region AB, the electrode voltage (b) increased in spite of a decreasing of the electrode current, clearly showing the negative resistance characteristics. We also ramped up the electrode current and observed the same negative resistance characteristics, and we observed the hysteresis in a curve of the stored energy versus input power due to L to H and H to L transition path [22]. These phenomena show that the bifurcation mechanism, accompanied with H mode transition, occurred in our electrode biasing experiments on the TU-Heliac. From Fig. 4, the improved mode continued until ~7 msec, because the line density (d) was sustained high level and the fluctuation level of the floating potential (f) and that of the ion

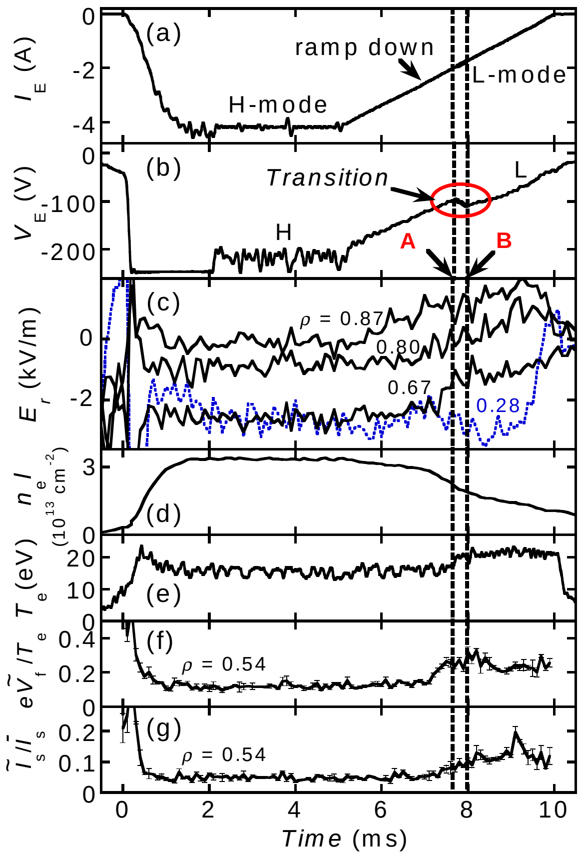

FIG. 4. Typical time evolution of (a) electrode current, (b) electrode voltage, (c) radial electric fields, (d) electron line density, (e) electron temperature, (f) floating potential fluctuation level, (g) ion saturation current fluctuation level.

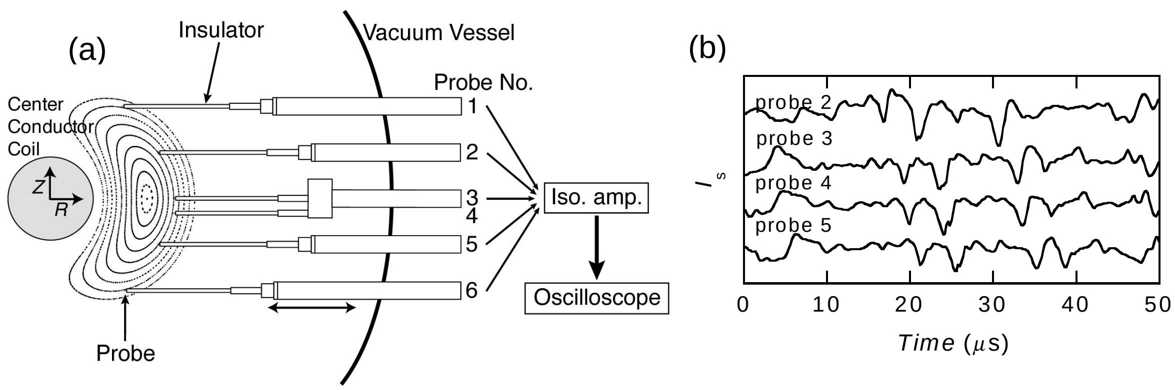

FIG. 5. The experimental set up of (a) a multi-Langmuir probe and (b) the time traces of ion saturation fluctuation signals in probe 2~5.

saturation current (g) were suppressed. Even in electrode *current sweep* experiments, these behaviors also showed the same characteristics as those of H-mode in large tokamaks and stellarators.

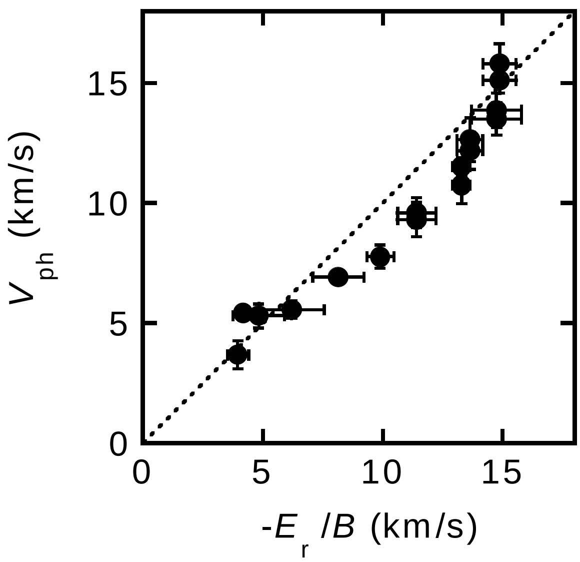

FIG. 6. The comparison between the rotation speeds estimated from the phase velocities of fluctuations in ion saturation current and the ***E×B*** *drift velocity where the electric field* ***E*** *was measured by the triple probe.*

Active control of the $\boldsymbol{J} \times \boldsymbol{B}$ driving force for the poloidal rotation by externally controlled electron injection was also demonstrated by measuring the fluctuation level of ion saturation currents by a multi-Langmuir probe shown in Fig. 5 (a). The radial positions of all tips of a multi-Langmuir probe were aligned along a same magnetic surface, and were calibrated by a low energy electron beam launched from an electron gun. The time traces of the ion saturation fluctuation signals in probe 2~5 are shown in Fig. 5 (b). The FFT analysis showed that the frequency range spread from 80 kHz to 130 kHz. From Fig. 5 (b) it is clear that all signals were kept a similar time evolution and had a phase shift according to the poloidal angles. Therefore we estimated the poloidal rotation speeds from the phase shift assuming that these fluctuations were conserved against a fluid rotation. Figure 6 shows the comparison between the rotation speed thus estimated and the $\boldsymbol{E} \times \boldsymbol{B}$ drift velocity where the electric field $\boldsymbol{E}$ was measured by the triple probe. We can see that the both rotation velocities were widely changed by the actively controlled electrode current sweep and the rotation speeds estimated from fluctuations phase shift almost agreed with the $\boldsymbol{E} \times \boldsymbol{B}$ drift velocities. The difference between these velocities can be minimized if we take account of the ion diamagnetic drift velocity, assuming $T_i = 0.1 - 0.5T_e$

4. Comparison between the Measured Damping Force and the Neoclassical Predictions

We estimated the ion viscous damping force from the driving force for the poloidal rotation and performed a comparison between the measured ion viscosity and the neoclassical predictions. In a steady-state, the driving force for the poloidal rotation balanced the ion viscous damping force and friction on the neutral particles. The surface averaged poloidal component of the momentum balance equation in toroidal geometry (ρ, θ, ϕ) can be written as follows [16, 23]:

$$< j_\rho > B_0 = -\frac{< B \cdot \nabla \cdot \Pi_\mathrm{i} >}{\Theta B_0} - (1 + 2q^2) n_\mathrm{i} m_\mathrm{i} \nu_\mathrm{in} V_\theta \,, \qquad (1)$$

where $V_\theta \equiv <(B_0/B_\phi)U_\theta> = \Theta V_\phi - E_\rho/B_0 + (1/n_\mathrm{i}Z_\mathrm{i}eB)\partial p_\mathrm{i}/\partial\rho$, $V_\phi \equiv <(B_0/B_\phi)U_\phi>$, $\Theta \equiv B_\theta/B_\phi$, $q \equiv \varepsilon/\Theta$, $\varepsilon \equiv \rho/R$ and < > denote surface average U, j, Π_i, B, E, and ν_in are the ion flow velocity, current density, ion viscosity stress tensor, magnetic field, electric field, and charge exchange collision frequency, respectively. B_0 is the field on the axis. n_i, m_i, p_i, and $Z_\mathrm{i}e$ are the ion density, mass, pressure, and charge, respectively. R and ρ are the averaged major radius and the minor radius, respectively. The left hand side of Eq. 1 indicates the driving force of $\boldsymbol{j} \times \boldsymbol{B}$ and the right hand side indicates the damping forces, *i.e.*, ion viscous damping force and friction on neutral particles. The heliac configuration has complicated magnetic Fourier components. The gradient of the ion temperature and that of the pressure weakly affect the magnitude of the ion viscosity and the helical ripple does not significantly affect the location of the local maxima of the viscosity [9, 24]. Therefore, the overall behavior of ion viscosity to the poloidal Mach number did not change, and therefore we considered only the toroidal ripple in the present study, neglecting the ion diamagnetic drift velocity and surface averaged toroidal flow. We adopted the plateau expressions in the Rozhansky model for a toroidal system [16] for ion viscous damping force and assumed the charge exchange process to be dominant collision with neutral particles. The schematic graph of the right hand side of Eq. 1 is shown in Fig. 7 where $M_p \equiv V_\theta/\Theta v_{th}$; poloidal Mach number and $v_{th} \equiv (2T_i/m_i)^{1/2}$; ion thermal velocity. The black solid and broken lines are the ion viscosity term and the friction term. The red solid line is the overall drag term.

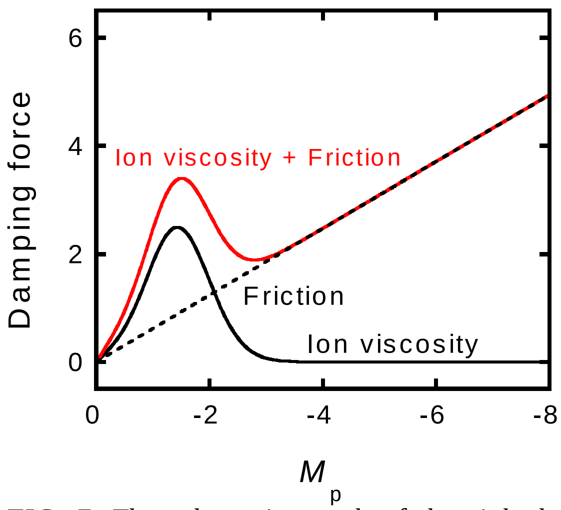

FIG. 7. The schematic graph of the right hand side of Eq. 1. The black solid and broken lines are the ion viscosity and the friction. The red solid line is the overall drag term.

In the region of the high poloidal Mach number, the dominant damping force on the poloidal rotation is the friction on neutral particles in TU-Heliac. We changed the filling pressure of the working gas He to change the collisionality. Figure 8 (a) shows the dependence of the electrode current on the electrode voltage at various filling gas pressures, $p = 0.7 - 5.4 \times 10^{-2}$ Pa. In all cases, the negative resistance region can be seen, which is enclosed by a circle. With regard to the transition conditions, V_E and I_E decreased with decreases in working gas pressure. The stronger E_r was formed with decreasing working gas pressure. The poloidal flow was formed easily in case of lower collisionality. In Fig. 8 (b), the vertical axis indicates the normalized driving force (L is the length of the magnetic axis), which corresponds to the left hand side of Eq. 2. Each symbol shows the surface averaged driving force estimated from the electrode current, and the horizontal axis indicates the poloidal Mach number estimated from the radial electric field. In these estimations, we assumed that the ion temperature T_i was $0.2T_e$. This assumption may be reasonable if the $\boldsymbol{E} \times \boldsymbol{B}$ rotating speed is equal to the experimental results of the Mach probe [21] and the result of the multi-Langmuir probe mentioned in the previous section. The solid and broken lines show the neoclassical ion viscous damping force including the friction term, which corresponds to the right hand side of Eq. 1. This damping force had a local maximum in the region $1 < -M_p < 3$, while in the high M_p region ($-M_p > 3$) the dominant damping force was friction and was linearly proportional to M_p. Figure 8 (b) clearly shows that the measured viscous damping forces had a local maximum at $-M_p \sim 1.5$ at all filling gas pressures and agreed well with the neoclassical predictions at low pressures, *i.e.*, in case of lower collisionality. However, at high pressures, differences were observed between the experimental results and theoretical curves. These differences may have been due to ambiguity in the charge exchange cross-section adopted in the present study. The plasma showed negative resistance characteristics (closed symbols) in the region where the neoclassical ion viscous

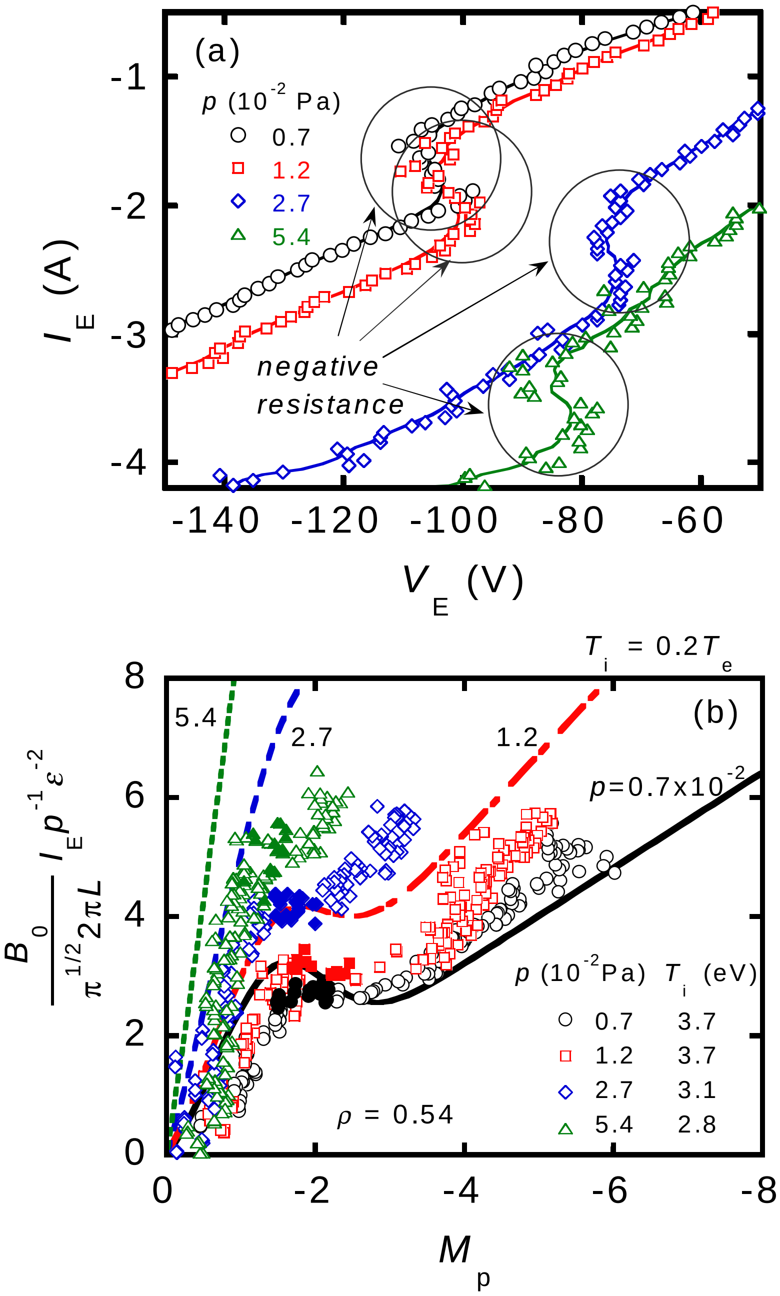

FIG. 8. (a) The dependence of I_E on V_E at various filling gas pressures p = 0.7 - 5.4 × 10^{-2} Pa. (b) The dependence of the measured damping forces (symbols) and the neoclassical damping force (broken and solid lines) on poloidal Mach number M_p. Closed symbols correspond to the negative resistance regions enclosed by circles in Fig. 8 (a).

damping force had a local maximum in $1 < -M_p < 3$ and the poloidal Mach number M_p corresponding to the negative resistance regions was independent of the working gas pressure, although the electrode parameters of the negative resistance regions were quite different. This suggested that the L-H transition occurred near the local maximum in ion viscosity which originates from a toroidal ripple [9].

5. Summary

The results of the biasing experiments using a hot cathode in the TU-Heliac can be summarized as follows: (a) The improved confinement mode, which has the same characteristics as those of H-mode in large tokamaks and stellarators, can be triggered with both *constant voltage* and *current sweep* biasing. (b) we can actively control the $\boldsymbol{J} \times \boldsymbol{B}$ driving force for the poloidal rotation by externally controlled electron injection using the *current-control* power supply. (c) Negative resistance features were observed between the electrode current and voltage at a wide range of filling pressure. (d) The measured damping forces had a local maximum at the poloidal Mach number M_p ~ 1.5, without regard to collisionality, and they agreed well with the neoclassical predictions of the Rozhansky model under the assumption $T_i = 0.2T_e$. (e) The plasmas showed negative resistance characteristics in the region where the ion viscous damping force had a local maximum.

The authors are grateful to Dr. K. Itoh, Dr. Y. Kamada and Dr. Y. Miura for helpful discussions. This work was supported in part by the LHD Joint Planning Research program at National Institute for Fusion Science.

References

[1] F. Wagner *et al.*, Phys. Rev. Lett. **49**, 1408 (1982).
[2] K. H. Burrell *et al.*, Phys. Rev. Lett. **59**, 1432 (1987).
[3] M. Kotschenreuther *et al.*, Phys. Plasmas **2**, 2381 (1995).
[4] V. Erckmann *et al.*, Phys. Rev. Lett **70**, 2086 (1993).
[5] K. Toi *et al.*, Plasma Phys. Control. Fusion **38**,1289 (1996).
[6] S.-I. Itoh and K. Itoh, Phys Rev. Lett. **60**, 2276 (1988).
[7] K. C. Shaing and J. E. C. Crume, Jr., Phys Rev. Lett. **63**, 2369 (1989).
[8] K. C. Shaing, Phys Fluids B **5**, 3841 (1993).
[9] K. C. Shaing, Phys Rev. Lett. **76**, 4364 (1996).
[10] R. J. Taylor *et al.*, Phys Rev. Lett. **63**, 2365 (1989).
[11] R. R. Weynants *et al.* Nucl. Fusion **30**, 945 (1990).
[12] L. G. Askinazi *et al.*, Nucl. Fusion **32**, 271 (1992).
[13] E. Y. Wang *et al.*, Nucl. Fusion **35**, 467 (1995).
[14] S. Inagaki *et al.*, Jpn. J. Appl. Phys. **36**, 3697 (1997).
[15] H. Dahi, J. N. Talmadge, and J. L. Shohet, Phys Rev. Lett. **80**, 3976 (1998).
[16] V. Rozhansky and M. Tendler, Phys. Fluids B **4**, 1877 (1992).
[17] S. Kitajima *et al.*, Jpn. J. Appl. Phys. **30**, 2606 (1991).
[18] S. Kitajima *et al.*, J. of Plasma and Fusion Research SERIES **4**, 391 (2001).
[19] K. Sawada, private communication.
[20] Y. Tanaka and S. Kitajima *et al.* to be published at JPFR SERIES **6** [Proc. ITC13].
[21] S. Kitajima *et al.*, Int. J. Appl. Electromagnetics and Mechanics **13**, 381 (2002).
[22] H. Takahashi *et al.*, presented at ICPP2004 [Nice, Oct. 25-29, 2004].
[23] J. Cornelis *et al.*, Nucl. Fusion **34**, 171 (1994)
[24] H. Takahashi and S. Kitajima *et al.* to be published at JPFR SERIES **6** [Proc. ITC13].